X-HALE AUTOPILOT WITH STABILITY AUGMENTATION AND SHAPE CONTROL BASED ON LOOP SEPARATION

Pedro J. González, Antônio B. Guimarães Neto, Guilherme Chaves Barbosa, Rafael M. Bertolin, Flávio J. Silvestre[1] and Carlos E. S. Cesnik[2]

[1]Department of Aerospace Engineering
Instituto Tecnológico de Aeronáutica
São José dos Campos, SP, 12228-900, Brazil
pgonzalez@ita.br, antoniobgn@gmail.com, rafaelmbufsj@gmail.com, guichavesbarbosa@gmail.com, flaviojs@ita.br

[2]Department of Aerospace Engineering
University of Michigan
Ann Arbor, Michigan, 48109-2140, USA
cesnik@umich.edu

Keywords: aeroservoelasticity, control of flexible aircraft, gain scheduling

Abstract: Highly-flexible aircrafts present high-aspect-ratio wings that introduce nonlinearities into the flight dynamics and make more complex models and control methods necessary. In this paper, a loop separation concept is applied to the X-HALE aircraft, giving rise to a control system comprising an inner-loop capable of controlling the shape of the aircraft while keeping the plant stable, and an outer-loop capable of controlling velocity, altitude, bank angle and sideslip angle. The outer-loop has a decoupled structure for longitudinal and for the lateral-directional axes. The matrices of the compensators were obtained using non-smooth optimization. Gain-scheduling techniques are implemented to bypass stability problems arising from changes in the plant with flight speed. Nonlinear simulations show promising results for implementation on the real aircraft.

1 INTRODUCTION

HALE (high-altitude long-endurance) aircraft are well known for their typical high-aspect-ratio wings, which make long-endurance flights feasible. The significant increase in the aspect ratio introduces high levels of structural flexibility and nonlinearities to such aircraft, imposing the need for flight-dynamic models that dynamically couple large rigid-body and large aeroelastic motions [1]. HALE wings can have their shapes significantly varied when the trimmed flight condition changes or when disturbances excite the aircraft.

The development of control systems for highly-flexible aircraft then requires more complex models and control techniques than those adopted for slightly-flexible aircraft. Classically, control law design is made assuming a rigid airframe, and aeroelastic interaction effects are only considered *a posteriori*, typically through gain stabilization, using low-pass and notch filters [2]. However, as the structural flexibility increases, notch filtering can become problematic for the control system performance [3]. With the separation of rigid-body and aeroelastic motions impossible, other strategies must be considered in designing control systems for highly-flexible aircraft.

An excellent example to demonstrate these concerns is the University of Michigans (UM) X-HALE [4], a flying testbed that behaves itself as a moderate flexible aircraft in its 4-meter-wingspan configuration with aspect ratio 20, but becomes highly flexible in its 6-meter-wingspan configuration with aspect ratio 30. The vehicle has been built at ITA in Brazil and is currently being used for validation of coupled models of flight mechanics and aeroelastic dynamics, and for flight control law design [5].

One alternative to address the airframe flexibility in the control law design is to add in the stabilizing inner-loop a shape control function with feedback of structural behavior [5]. The idea behind that is to artificially make the aircraft behave as a slightly flexible aircraft, so that rigid-body-based outer-loops for path tracking apply. However, stability margins may decay as the flight condition changes. For higher flight speeds, the demanded deflections of control surfaces by the shape control function may be excessive and lead to instabilities of aeroelastic modes. A gain-scheduling approach is therefore needed.

In this paper, a flight control law based on the loop separation concept and a shape control function is addressed for longitudinal and lateral-directional dynamics of a highly flexible aircraft. The performance of the control law and the decay of stability margins with increasing flight speed is demonstrated for the X-HALE aircraft. Gain-scheduling techniques are discussed and implemented in nonlinear closed-loop simulations. Results show that a computationally-efficient gain-scheduling approach stabilizes the plant in the flight speed range of interest, and its implementation on the real aircraft is promising.

2 MODEL DESCRIPTION AND CONTROL SYSTEM STRUCTURE

The X-HALE wing is built connecting six panels one-meter-span by 0.2 meter of chord panels, with the external panels having dihedral of 10°. Figure 1 shows the X-HALEs geometry. The aircraft has five under-wing-mounted pods for the installation of the instrumentation. Five horizontal stabilizers are present, connected to the wing with booms. The central and the two inner booms have ventral fins for lateral-directional stability.

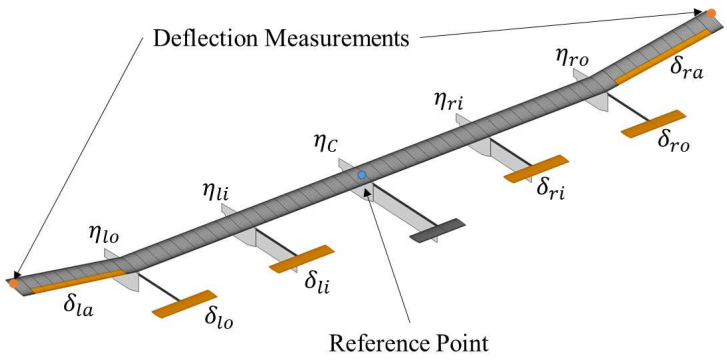

Figure 1: X-HALE geometry, control surfaces and reference points.

A camera system was proposed for measuring the elastic deformation of the wing [6]. The cameras are installed on the central pod facing outwards. A set of LED markers is installed on

the upper surface of each wing panel. The camera system is capable of detecting the displacement and rotation of these markers. This technique is being adapted for use in real-time control applications [6].

X-HALEs flight dynamics model is based on the formulation developed by Guimarães Neto *et al* [7] for the flight dynamics of slightly- to moderately-flexible aircraft. Small elastic deformations are assumed. A finite-element representation of the aircraft structure and a lumped-mass representation of its properties of inertia is available to characterize the structural dynamics. Incremental unsteady aerodynamics is modeled using the doublet-lattice method [8] with rational function approximations [9] and appropriate aerodynamic influence coefficient corrections to take into account viscous effects.

The resulting flight-dynamic model of the X-HALE comprises 222 states, and the basic trimmed level-flight condition is obtained for the design flight speed of 14 m/s at 700 m ISA altitude. The linearization of the aircraft dynamics around the equilibrium condition produces the matrices that are to be used in the design of the control system. The operation heights for X-HALE goes from 700 to 800 m, the initial height is the altitude of São José dos Campos (local for the flight tests). The flying velocities range goes from 12 m/s to 20 m/s based on the take off speed and the performance of the engines.

2.1 The control law: stabilizing loop (inner-loop)

The control system inner-loop must ensure that all closed-loop poles lie in the left half-plane, using the lowest possible control energy and leading to adequately-damped aircraft response. It comprises a stability augmentation system (SAS) for the global motion of the aircraft and a shape control function, as proposed by González *et al* [5].

For the stability augmentation of global motion, pitch attitude θ and roll angle ϕ and the angular rates p, q, and r are measured outputs used in the feedback loop. Elastic vertical translations of the reference points on the wing tips (see Fig. 1) complete the inner-loop to enhance shape control. The inner-loop has 9 gains: 5 for the rigid body stabilization and 4 for shape control. The proportional gains were calculated using Linear Quadratic Regulator (LQR) with output feedback.

LQR control technique applies to linear systems of the form

$$\begin{aligned} \dot{x} &= Ax + Bu \\ y &= Cx, \end{aligned} \tag{1}$$

$x \in R^n$ is the state vector, $u \in R^m$ is the control input and $y \in R^p$ is the measured output [10]. The control signal is the output feedback given by

$$u = -Ky, \tag{2}$$

and the close-loop system is defined as

$$\dot{x} = (A - BKC)x = A_c x. \tag{3}$$

The LQR allows to calculate the feedback gain matrix K by minimizing the performance index J, a cost function defined as

$$J = \frac{1}{2}\int_0^\infty (x^T Q x + u^T R u)dt. \tag{4}$$

Q is a positive semidefinite state weight matrix and R is a positive definite control weight matrix.The pair (Q, R) is required to be detectable, but observability may be proved instead. The necessary conditions to solve the LQR are given by two Lyapunov equations and a third equation to obtain K. [10]

$$0 = A_c^T P + P A_c + Q - P C R^{-1} C^T P, \tag{5}$$

$$0 = A_c S + S A_c^T + X, \tag{6}$$

$$K = R^{-1} B^T P S C^T (C S C^T)^{-1}. \tag{7}$$

It is required to solve these three equations coupled to obtain a gain capable to minimize J. If the system is stable, J could be written as

$$J = \frac{1}{2} x^T(0) P x(0) = \frac{1}{2} tr(PX). \tag{8}$$

Once a stabilizing gain is obtained by minimizing the maximum real part of the eigenvalues of A_c. The system of equations (5-7) is solved numerically in an iterative process to minimize J in Eq. (8) [10].

In the inner-loop structure, the two inboard elevons δ_{li} and δ_{ri} are actuated symmetrically for the longitudinal feedbacks of θ and q, the outboard elevons (δ_{lo}, δ_{ro}) are actuated anti-symmetrically for the lateral-directional feedbacks of ϕ, p and r. Simultaneously, shape control is achieved using the ailerons (δ_{la}, δ_{ra}) of the left and right external wing modules. The described approach results in a symmetric and independent decoupled matrix for shape control and a decoupled matrix for stability augmentation around a trimmed level-flight condition. The strategy of decoupling the gain matrix and ensuring symmetry/anti-symmetry on the control commands is based on a physical consideration that the aircraft is nearly symmetric. It produces lower performance indexes and improves time domain responses.

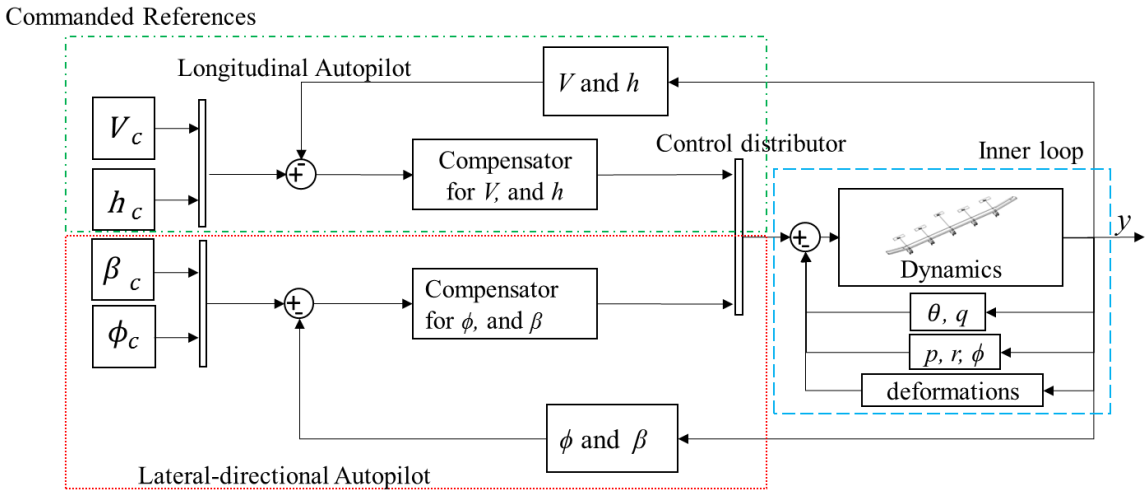

Figure 2: Control system structure, with stabilizing inner-loop and tracking outer-loops.

2.2 The control law: tracking loop (outer-loop)

The outer-loop has the structure of a regular tracker autopilot [10]. Two tracking compensators were developed; a longitudinal tracking controller for velocity and altitude, and a lateral-directional tracker for bank angle and sideslip angle regulation. The complete control system with inner- and outer-loop can be seen in Fig. 2.

The reference input is given by

$$z = H_a x \tag{9}$$

where z is a vector with the variables to be tracked: velocity (V) and altitude H_a for the longitudinal motion, and sideslip (β) and bank angle (ϕ) for the lateral-directional motion. The dynamic compensator has the form

$$\begin{aligned} \dot{w} &= Fw + Ge \\ u_v &= Dw + J_c e, \end{aligned} \tag{10}$$

with state (w) and output (u_v). The tracking error e is

$$e = r - z, \tag{11}$$

where r is a vector with references to be tracked. F, G, D and J_c are matrices selected to include the desired structure in the compensator. The commands of outer- and inner-loops are the final control input

$$u = -Ky - u_v. \tag{12}$$

The whole system could be written in its augmented form as

$$\frac{d}{dt}\begin{bmatrix} x \\ w \end{bmatrix} = \begin{bmatrix} A & 0 \\ -GH_a & F \end{bmatrix}\begin{bmatrix} x \\ w \end{bmatrix} + \begin{bmatrix} B \\ 0 \end{bmatrix} u + \begin{bmatrix} 0 \\ G \end{bmatrix} r, \tag{13}$$

$$\begin{bmatrix} y \\ u_v \end{bmatrix} = \begin{bmatrix} C & 0 \\ -J_c H_a & D \end{bmatrix}\begin{bmatrix} x \\ w \end{bmatrix} + \begin{bmatrix} 0 \\ J_c \end{bmatrix} r, \tag{14}$$

$$z = \begin{bmatrix} H_a & 0 \end{bmatrix}\begin{bmatrix} x \\ w \end{bmatrix}. \tag{15}$$

and the total control input is

$$u = -\begin{bmatrix} K & I \end{bmatrix}\begin{bmatrix} y \\ u_v \end{bmatrix}. \tag{16}$$

In summary, the augmented, closed-loop system has the form

$$\begin{aligned} \dot{x_a} &= Ax_a + B_a u_a + Gr \\ y_a &= Cx_a + Fr \\ u &= -\begin{bmatrix} K & I \end{bmatrix} y_a, \end{aligned} \tag{17}$$

Matrices F, G, D and Jc defining the structure of the compensator were determined via a structured non-smooth H_∞ synthesis, that is detailed in the following.

2.3 Non-smooth H_∞ Synthesis

The closed-loop system can be represented by the Linear Time Invariant (LTI) P_G of Eq. (18), with subscript a indicating augmented states and matrices. [11]

$$P_G = \begin{cases} \dot{x}_a = Ax_a + B_a u_a + G_a r \\ z = H_a x_a \\ y_a = C_a x_a + F_a r \end{cases} \tag{18}$$

Closing the loop with the control law $u = -[I]y_a = -y_a$, the closed-loop transfer function between tracking error e and control (output) u is a function of the plant and the augmented compensator,

$$T_{ue} = F_l(P_G, F, D, G, J_c). \tag{19}$$

The objective is to compute the longitudinal and lateral compensators. The compensators must be able to attain three requirements: performance, compensator stability and global stability [12]. The performance is attained by finding the matrices F, D, G, J_c that minimize the H_∞ norm of the function T_{ue}

$$\|T_{ue}(P_G, F, D, G, J_c)\|_\infty = \sup \overline{\sigma}(T_{ue}(j\omega)), \tag{20}$$

where ω is the banwidth. The advantage of structured H_∞ is to freeze the control architecture and the order of the compensator for V-h and β-ϕ. [12]. In the longitudinal compensator the two central elevators control the aircraft speed, meanwhile, all engines actuate together to attain the commanded altitude . In the lateral-directional compensator the sideslip angle is regulated by the action of the differential thrust of the outer engines acting a pair minus the other, the bank angle is controlled with the two outer elevators acting differentially. The architecture of both compensators is

$$F = F_{4\times4}, G = G_{4\times2}, D = D_{2\times4}, J = J_{2\times2}. \tag{21}$$

A critical factor is decoupling the action of the controllers inside the compensators. Equation (21) shows a system with two inputs and two outputs with two controllers acting and four controller states. It is important that the action of one pair of controllers have little or no effect over the other.

Regular H_∞ synthesis uses semi-definitive programming or algebraic Ricatti equations to compute the feedback controllers [11] . When we fix the structure of the controller, i.e. the order of the controller state-space realization, the H_∞ synthesis problem is no longer convex. Normally, when this problem exists the Bounded Real Lemma is used [13]. As a result the H_∞ synthesis no longer produces LMIs, but bilinear matrix inequalities, which are non-convex. This approach usually leads to numerical difficulties because of the presence of Lyapunov variables, whose number grows quadratically with the number of states.

The non-smooth approach does not use the Bounded Real Lemma and avoid Lyapunov variables. The algorithm presented by Apkarian and Noll [11] evaluates the H_∞-norm with the Hamiltonian bisection algorithm and uses it to compute subgradients. These subgradients are used to compute the descent steps. This algorithm is available in the Matlab routine Looptune [14].

Looptune is a function of MATLAB Robust Control System Toolbox that computes the Clarke subdifferential [11], [15] to solve the H_∞-norm problem adapted to a finite number of frequencies. [14]. Requirements of tracking, stability margins and compensator stability are formulated in the frequency domain by H_∞ constrains of the form

$$\|WT\|_\infty < 1. \tag{22}$$

T is the transfer function of interested variables, W is the weighting function describing the expected performance. For the X-HALE control system, multiple performance constraints were required. The constraints are inserted on the optimization problem with the TuningGoal function of Matlab. First, all compensators poles must be stable (all poles must be negative) and the performance of the output signal should have a 6 db gain margin and 45 degrees phase margin for all outer-loop feedbacks, as stated in MIL-DTL-9490E [16]. The procedure in Looptune leads to finding a stabilizing controller that satisfies the set of H_∞ constrains

$$\|W_i T_i\|_\infty < 1, i = 1, ..., m. \tag{23}$$

The weighting functions are filters that define the form of the sensitivity function $S = 1 - T$. The weight is defined with

$$W_S = \frac{\frac{s}{M_\omega} + \omega}{s + \omega A_\omega}, \tag{24}$$

A_ω is the lower bound and M_ω the upper bound for the sensitivity. The structured H_∞ synthesis allows to concatenate the H_∞ constraints in the generalized form

$$\|H\|_\infty < 1 \tag{25}$$

where

$$H = diag[W_1 T_1, ..., W_m T_m] \tag{26}$$

Then, the nonsmooth optimization included in the structured H_∞ methods is capable to optimizing the entire constraint H instead of the global transfer function. An iterative process was developed to construct a proper controller. The constraints applied over the $T_{ue}(P_G, F, D, G, J_c)$ functions were set between 0.5 and 5.65 rad/sec to avoid affecting the inner-loop rigid body dynamics ($\omega \gg$ 0.01 Hz) while also avoid the first elastic mode frequency ($\omega <$ 0.9 Hz). The final bandwidth for the longitudinal compensator is [0.94 rad/s, 1.41 rad/s]. The same principle

was used for the lateral-directional compensator, its final bandwidth is [1.48 rad/s, 3.53 rad/s]. These frequency settings offered the best time domain response, they also showed low coupling inside the compensators.

Figure 3 and 4 show the requirements for both compensators. It is possible to see that in both cases the final compensators are stable. All poles rest on the left side of the imaginary axis.

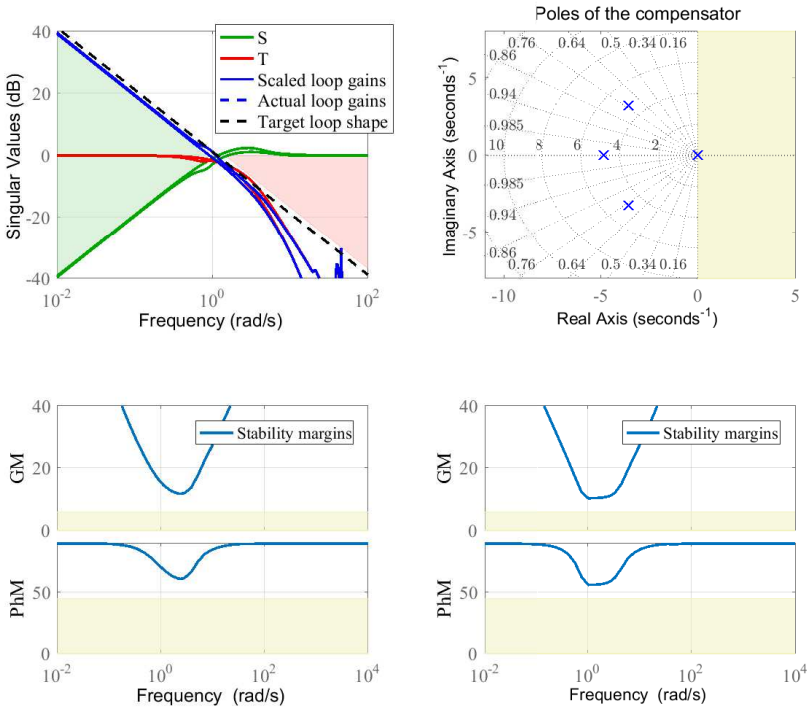

Figure 3: Review of the requirements for the longitudinal compensator.

Figure 3 bottom left Bode plot of the transfer function between the velocity and the central elevators and bottom right shows the transfer function between the directional control input (engines) and the altitude. It is possible to see how in both cases the requirements for phase margin (PhM) and gain margin (GM) were attained. TuningGoal.LoopShape of Matlab constrains the open-loop response L (Loop gains). The objective open-loop gain profile is transformed into constraints on the inverse sensitivity function and the complementary sensitivity function

$$\begin{aligned} inv(S) &= I + L, \\ T &= 1 - S. \end{aligned} \tag{27}$$

The green shaded region in Fig. 3 and 4 represents the area where L is much greater than 1. Here a constraint on $inv(S)$ is the same applied to a minimum constraint on L. A large L is associated to good disturbance rejection, good command following and stabilization [17].

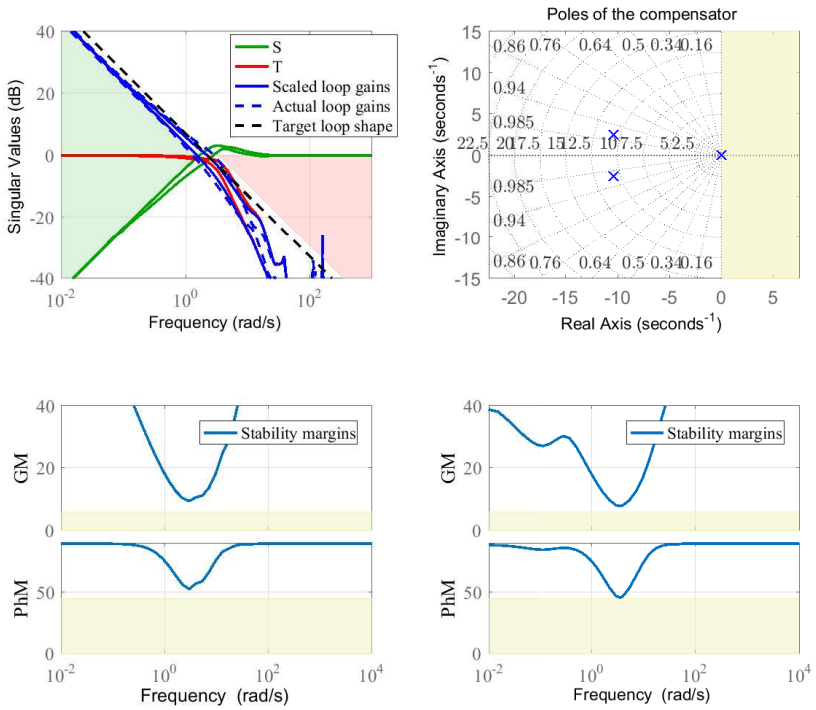

Figure 4: Review of the requirements for the lateral-directional compensator.

The red shaded region shows the area were L is much smaller than 1. Here a maximum gain constraint on the consensitivity is the same to a maximum gain constraint on L. A small L is associated with noise mitigation and small magnitude of input signals [17] .The space between these two regions is twice the bandwidth set as initial requirement and specifies the frequency band were the loop gain is able to cross 0 dB. At the center of the singular values plot on Fig. 3 it is possible to see that the cut bandwidth limits for L were achieved and the constraints limits were respected.

The bottom left and bottom right Bode plots show the transfer function between the directional control input (external engines) and β, and the mixed outer elevators and ϕ respectively. Once again is possible to see how the requirements in terms of PhM and GM were attained. The plots also shows that the cut frequency bandwidth for L was respected. It is possible to observe that the constraints are not respected at a high-frequency point by the actual loop gain. Nevertheless, it is at so high frequency that it does not affect the general performance of the lateral compensator as is shown in the next section.

3 CONTROL SYSTEM EVALUATION

The control system described in the last section was applied to X-HALE for nonlinear, closed-loop simulations to assess its performance. The maneuver consists in a climbing turn. The commands are: an increment of 20 m height, velocity increment of 4 m/s and 20 degrees in roll angle in 40 s, while β is regulated to zero. Figure 5 shows nonlinear time domain responses to these commands.The increase of altitude was attained with zero percent of error at 40 s. The increase of velocity was also achieved at 40 s with zero overshoot. Steady state error is also considered zero. The roll angle reference is reached and the steady state error is 0.06 deg, meanwhile, the sideslip angle was regulated around zero, allowing the aircraft to perform a

coordinated turn. The maximum variation of the sideslip angle was -0.76 degree.

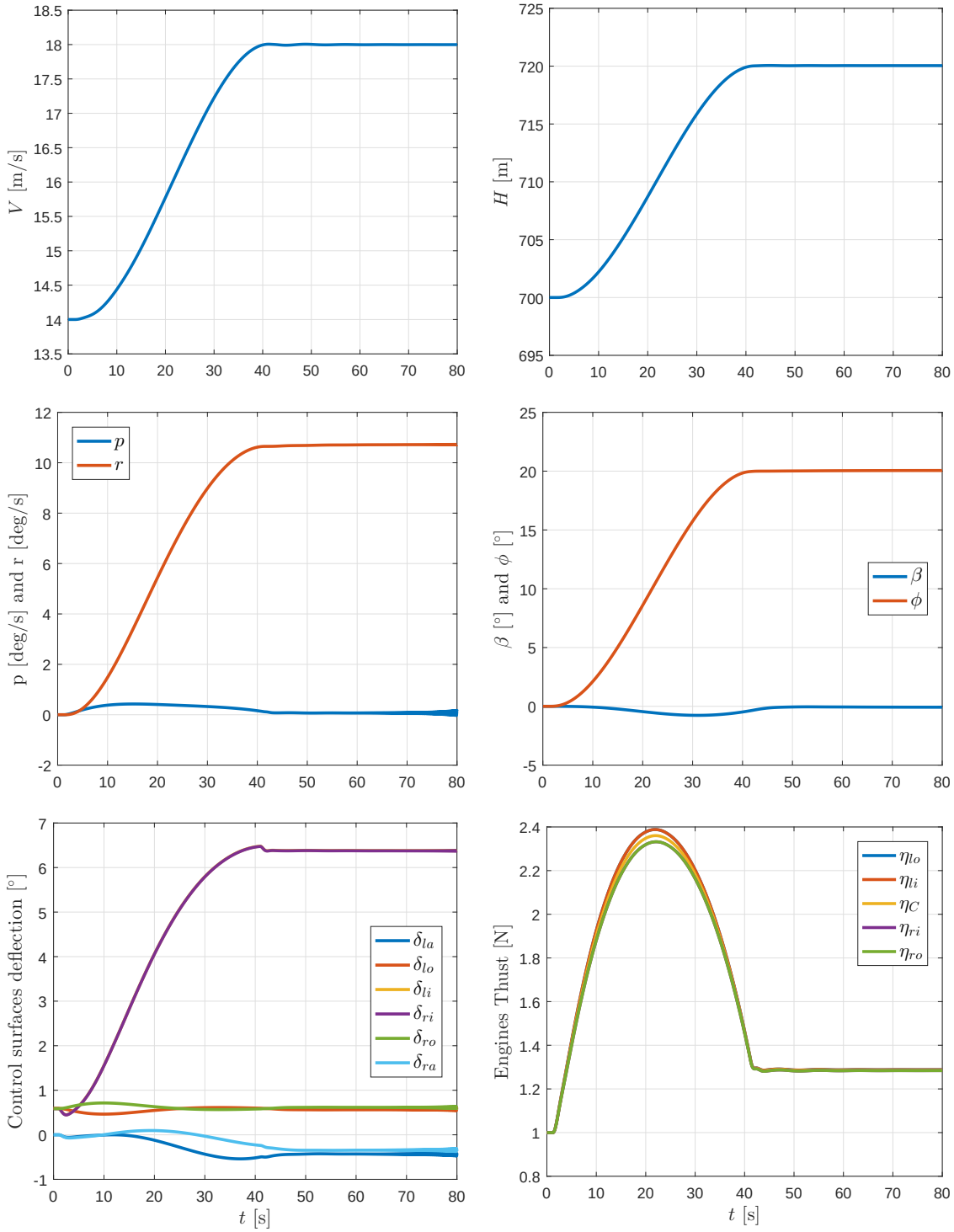

Figure 5: X-HALE nonlinear response time histories and variation of control inputs for the commanded maneuver.

One of the most interesting phenomena observed in the X-HALE ITA flight-dynamic model is that the aircraft presents lateral control reversal for the elevons. One can indeed observe in Fig. 5 that the left elevons are deflected upwards and the right elevons are deflected downwards for the aircraft to roll to the right, i.e. the opposite of a conventional aircraft. With the elevons installed at the tail of rather lengthy booms, an intense elastic twist occurs at the wing when the elevons are deflected. As a result, deflecting the left elevon upwards and the right elevons downwards to turn to the left has the effect of twisting the wing, increasing local angles of attack

of the left wing sections while the opposite occurs for the right wing sections. The consequence is an overall rolling moment to the right, the opposite of the desired. No control reversal exists for the ailerons, the closed-loop control system makes them deflect with the same sign, in order to reduce the wing bending deformation induced by the increased left wing lift and decreased right wing lift. The control surface deflections are far from the saturation limit of $\pm$ 25°. Once the commanded reference is reached the control surfaces keep acting to control the shape of the aircraft.

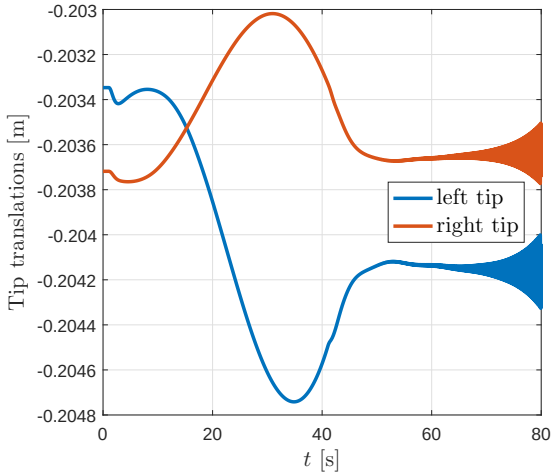

Figure 6: Vertical translations of the wing tips.

The variation of thrust is also within the limits of the engine's capabilities, as seen in Fig. 5 (bottom right plot). The engines increase thrust to attain the commanded altitude. The sideslip angle is regulated by the asymmetric thrust. After the commanded roll angle is attained the thrust remains constant to hold the coordinated turn.

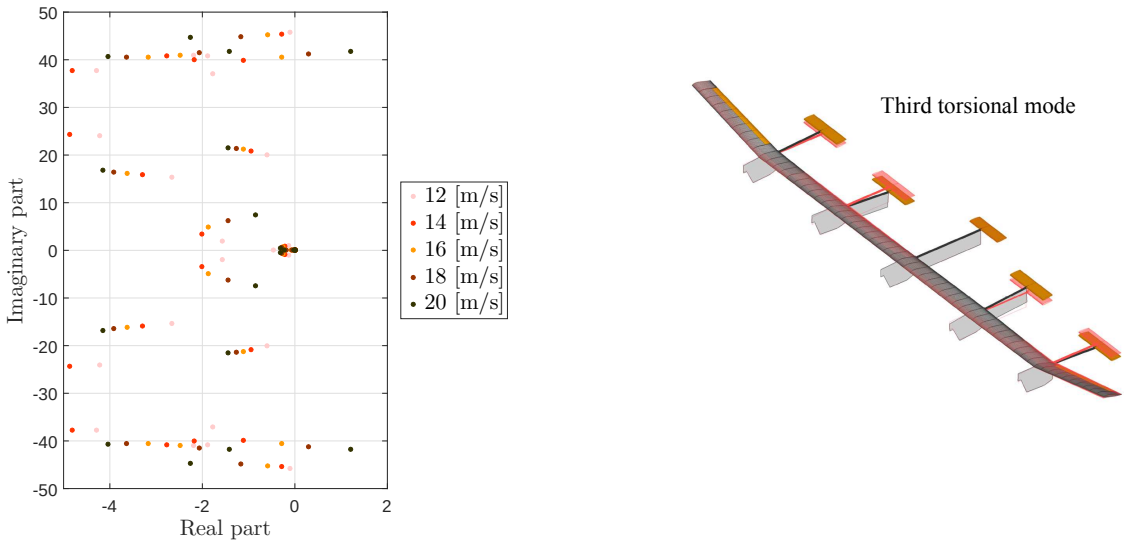

Figure 7: Variation of SAS poles as a function of velocity.

In Fig. 6, tip translations are displayed for the left and right wing. Right and left wings react differently entering the coordinated turn due to different local angles of attack resulting from the

twisting moment generated by the elevons. After 60 s, an instability shows up in both responses.

The instability is achieved when the third torsional mode poles cross the imaginary axis as seen in the closed-loop root loci of Fig. 7 for increasing velocity. The form of the mode is presented on the right side of Fig. 7. It is possible to see how the inner-loop calculated for 14 m/s keeps the airplane stable from 12 m/s up to approximately 17.5 m/s. Once this velocity is exceeded, the SAS is no longer capable of stabilizing the aircraft. In order to overcome this problem, the control system must be adapted to stabilize the aircraft in the whole flight envelope.

4 GAIN SCHEDULING

Results of last section have demonstrated that a fixed set of gains was not able to ensure stability over the entire X-HALE flight envelope. The system is dependent on the trimmed shape of the structure. Gain scheduling (GS) is used to solve this problem [18]. This technique consists in scheduling the gains of the controller according to changes in aircraft state [19], for instance the velocity. A series of inner-loops were designed for the LTI models linearized at 12, 14, 16, 18 and 20 m/s. Four approaches were taken to solve this problem: the first GS solution consists in designing the inner-loop for each LTI and generating a linear function to move from one set of gain to the next one; the second GS solution consists in keeping the inner-loop constant for the nearest speed switching every time the aircraft reaches a new linearized point; the third GS solution is a linear function between the sets of gains calculated for 14m/s and 18m/s;the fourth GS solution consists in a switch at 17 m/s that changes from the gains of 14 m/s to the gains of 18 m/s.

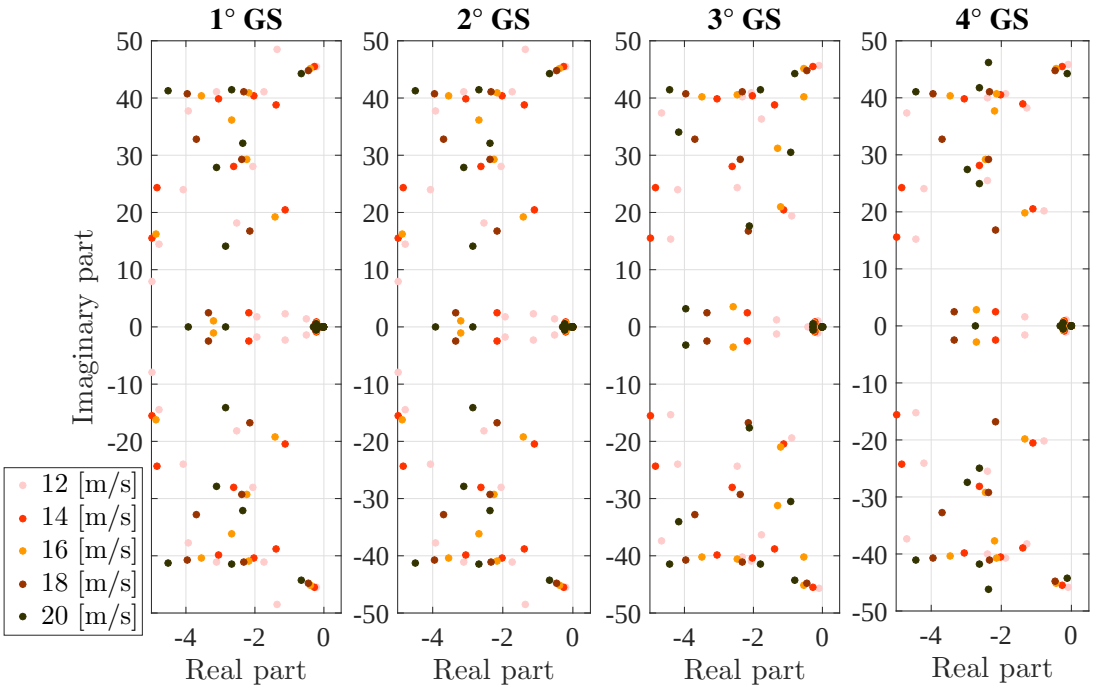

Figure 8: Variation of SAS poles as a function of velocity for all GS

In the first GS solution, the gains were stored in a lookup table and with the help of staggered

models, the gains were calculated every 0.1 m/s by linear interpolation. For a real implementation, however, a measurement of a 0.1 m/s variation in the flight speed is not possible with the current onboard instrumentation. In the second and fourth GS solutions, an algorithm was applied to check stability of the inner-loop, the gains were kept constant between a series of velocity strips of $\pm$ 0.5 m/s for the second case. The fourth case switches at 17 m/s. Once the aircraft passes one of the limits, the inner-loop gains are switched to the next set of gains. In this way, the stability of the inner-loop was granted to the entire flight envelope. Figure 8 displays the root-loci of the closed-loop system considering the four different strategies for gain-scheduling. The plots show clearly that the poles never pass to the right half plane for analyzed velocity.

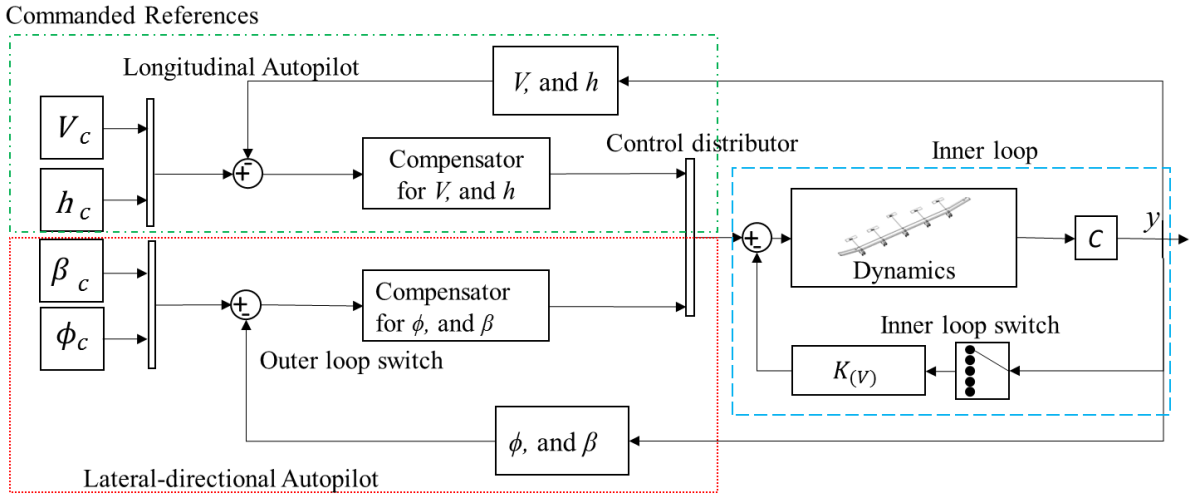

Figure 9: Control system structure with gain scheduling

The outer-loop was evaluated in order to check stability and efficiency. The longitudinal and lateral compensators were able to take the aircraft to all commanded references. The controller is robust enough to not lose significant performance during the entire flight envelope. In this way, the whole flight envelope of X-HALE is attained. Figure 9 shows the final control system for X-HALE with structural shape control and gain scheduling based on the loop separation concept.

5 RESULTS

The evaluation of the whole controller consists in a climbing accelerated turn. Departing from an initial velocity of 14 m/s to 18 m/s in 40 s, the commanded height variation was 20 m and the climbing time was 40 s, at the same time the aircraft was commanded to turn 20 degrees in roll angle and regulate sideslip angle. Figures 10 to 12 presents the results of the nonlinear simulations. The continuous lines represent the linear GS approaches (1° GS and 3° GS). The dotted lines represent the switching GS approaches (2° GS and 4° GS).

Figure 10 shows how the longitudinal commands are achieved with both GS approaches. Nevertheless, it is noted that the variation of the velocity is not as continuous as shown in Fig. 5. The 2° GS shows a higher frequency damped oscillation once the commanded velocity is achieved.

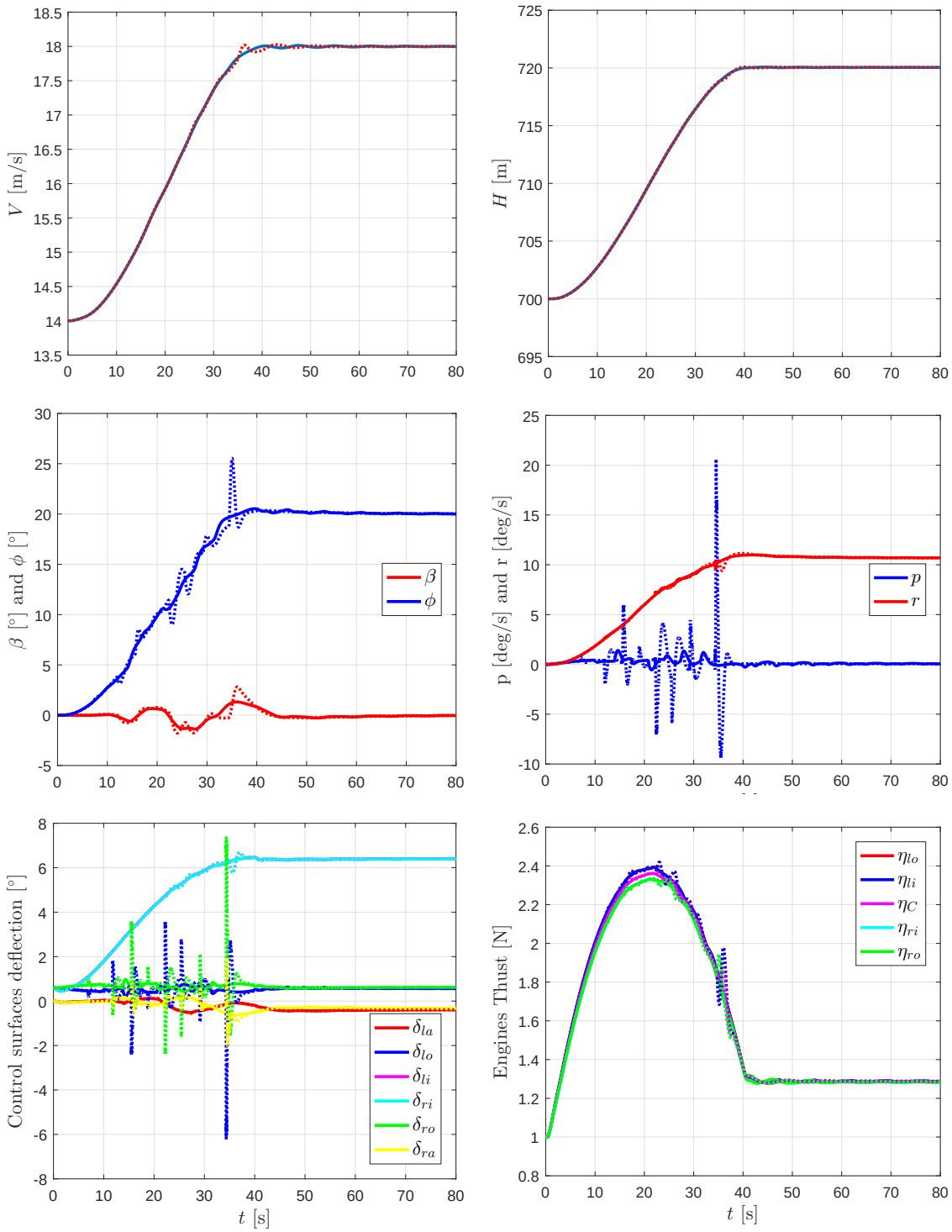

Figure 10: X-HALE nonlinear response time histories and variation of control inputs for 1° GS and 2° GS

The effect of consecutive gain switching is more visible on the lateral maneuvers. Every time that a set of gains is switched to another, there exists a jump in the control signal. These jumps are rapidly compensated by the outer-loop to sustain the maneuver. Nevertheless, there is no control saturation during the maneuver. The commanded roll angle presents an overshoot of 5 degrees just before attaining the stationary state reference for 2° GS. It is also evident that these jumps in the commanded signals generate actions on the aircraft that increase the control demand to attain the maneuver. The sideslip angle increases at the same time that the control jumps occur. The engines must act in order to try to reduce β while they are controlling the

climbing.

Plots of p and r in Fig. 10 show that the aircraft is no longer unstable at 18 m/s. Once the commanded references are attained, the aircraft is able to hold the maneuver, showing that the gain scheduling allows the controller to adapt itself to a new flight condition. It is also important to point out that the outer-loop does not loose significantly performance with the changes in the inner-loop. The outer-loop is capable of compensating the control variation due to the switching while tracking the references.

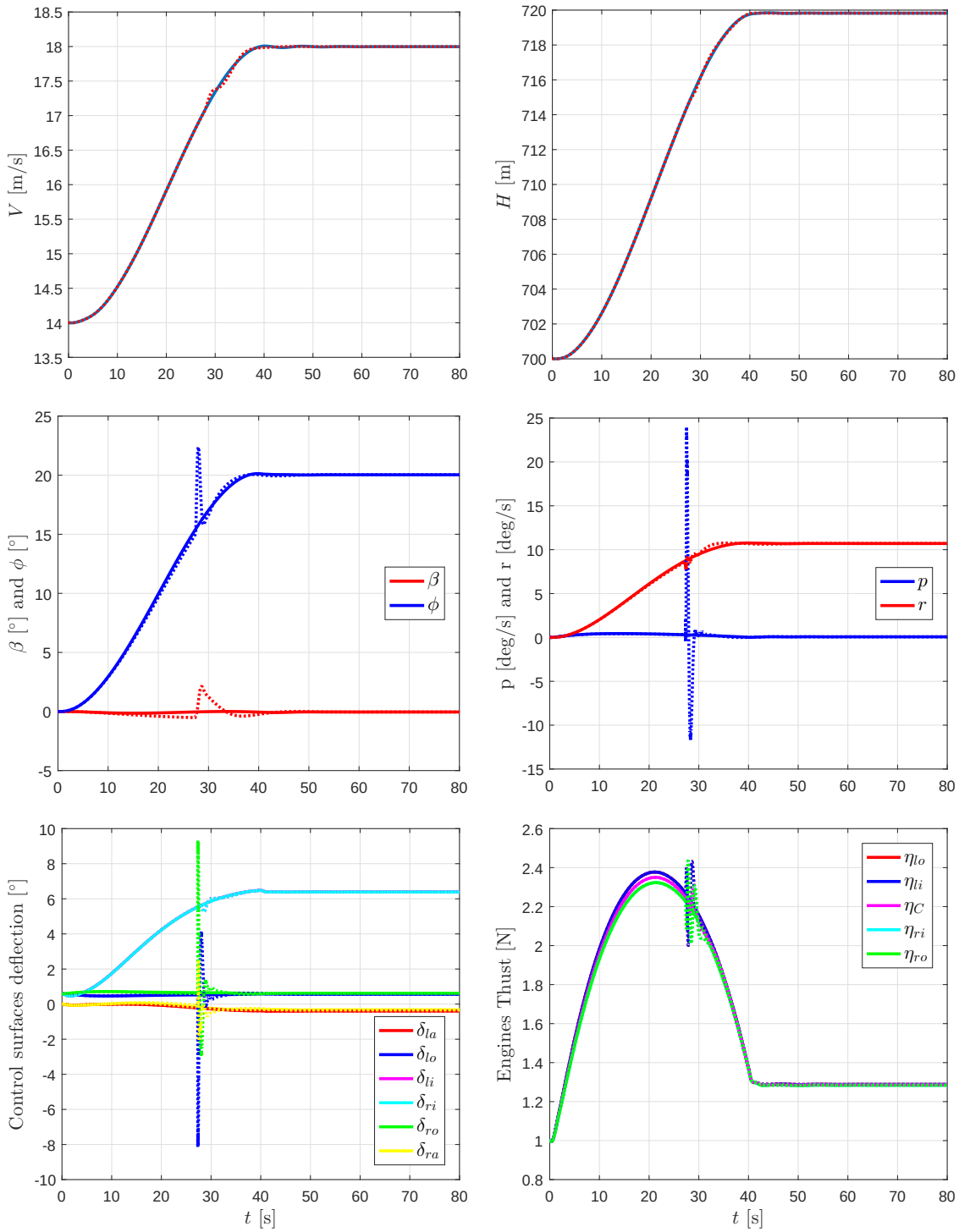

Figure 11: X-HALE nonlinear response time histories and variation of control inputs for 3° GS and 4° GS.

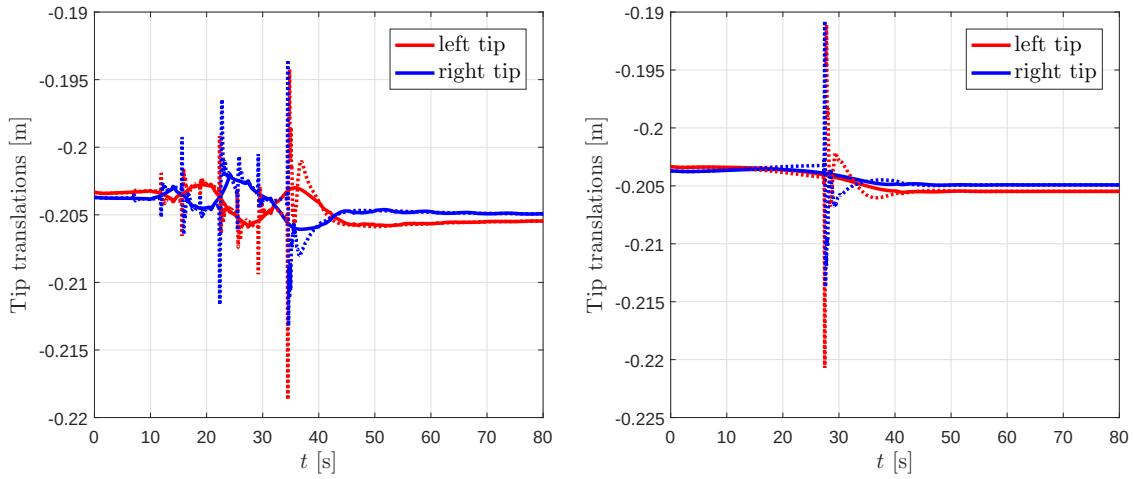

Figure 12: Vertical translations of the wing tips with Gain Scheduling. (1° GS and 2° GS (dotted) left, 3° GS and 4° GS (dotted) right)

Despite of that, the commanded references were attained and the steady-state tracking errors were small.

Nonlinear simulation results for 3° GS and 4° GS are shown in Fig. 11. The first remark from this figure is that the tracking is accomplished more smoothly, without much oscillation during the transition phase. At 17 m/s the inner-loop switch changes from the 14 m/s gain to the 18 m/s. This change on the inner-loop generates an increases in the control command which deflects the outer elevators to over $\pm$ 8 degrees. This causes an increase of ϕ angle to 22.38 deg. This variation is rapidly compensated by the outer-loop and returns X-HALE to the tracking reference. The variation of roll angle induces an increase in β, this variation is regulated by the engines without loosing performance during the climbing, a small variation is observed in the 4° GS in the velocity tracking. The 3° GS presents the best response of the four GS evaluated. All commanded references were attained without any overshoot or significant steady-state error. The transition between the inner-loop gains is achieved smoothly. The coordinated turn is achieved and stable stationary roll and yaw rates are observed.

Finally, Figure 12 shows the variation of the wing tip of X-HALE during the maneuver with the four GS approaches. It is possible to observe that the aicraft is stable, and the aeroelastic instabilities shown in Fig.6 were eliminated. The, 3° GS approach is able to take the aircraft through the entire maneuver without discontinuities in the response, from the initial deformation condition to a new trimmed one.

6 CONCLUSION

A control law based on wing deformation measurements was designed and applied to a highly flexible aircraft. The control architecture was based on loop separation concept. The inner-loop was in charge of stabilizing and holding the trimmed shape of the aircraft. Meanwhile, the outer-loop was used to track commanded references. The inner-loop is decoupled, in terms of longitudinal and lateral-directional global motions. The shape of the aircraft is controlled, with one half-wing independent from the other. The gains of all control surfaces are symmetric. The inner-loop was estimated by LQR with output feedback, and its architecture allows the aircraft to hold the equilibrium condition and wing shape with low control energy.

Decoupling the inner-loop allows the outer-loop to be split into two independent loops. The

longitudinal loop controls velocity and height and the lateral-directional loop controls roll angle and sideslip angle. The optimization of the compensators used to follow the references was achieved by nonsmooth H_∞ synthesis. In general, commanded references were attained with no control saturation and small tolerable steady-state errors. However, since the plant is highly dependent on flight velocity, large variations on commanded reference velocities resulted in instability for a fixed gain set.

Gain scheduling of the inner-loop was necessary to ensure stability. Nonlinear results showed clearly that switching gains may decrease the performance in closed-loop, and additional oscillations appear in the response. Gain optimization process may lead to local minimums that changes the values of the gains considerably compared to the gains found for subsequent velocities. This causes the jumps observed in the results. The 3° GS approach was demonstrated to hold stability while conferring the aircraft smooth responses throughout the speed range.

Thanks to its simplicity and robustness this control architecture shows promising results for implementation on the real X-HALE.

7 REFERENCES

[1] Cesnik, P. R., C. E. S. and Reichenbach, E. (2014). Reexamined structural design procedures for very flexible aircraft. *Journal of Aircraft*, 51(5), 1580–1597.

[2] Abzug, M. J. and Larrabee, E. E. (2005). *Airplane stability and control: a history of the technologies that made aviation possible*, vol. 14. Cambridge University Press.

[3] Silvestre, F. J., Guimarães Neto, A. B., Bertolin, R. M., et al. (2016). Aircraft control based on flexible aircraft dynamics. *Journal of Aircraft*, 54(1), 262–271.

[4] S. Cesnik, C. E., Senatore, P. J., Su, W., et al. (2012). X-hale: A very flexible unmanned aerial vehicle for nonlinear aeroelastic tests. *AIAA journal*, 50(12), 2820–2833.

[5] González, P. J., Silvestre, F. J., Paglione, P., et al. (2016). Linear control of highly flexible aircraft based on loop separation. In *AIAA Atmospheric Flight Mechanics Conference,*. pp. 10.2514/6.2016–3398.

[6] Pang, Z. Y., Cesnik, C. E., and Atkins, E. M. (2014). In-flight wing deformation measurement system for small unmanned aerial vehicles. In *55th AIAA/ASMe/ASCE/AHS/SC Structures, Structural Dynamics, and Materials Conference*. pp. 10.2514/6.2014–0330.

[7] Guimarães Neto, A. B., Silva, R. G., Paglione, P., et al. (2016). Formulation of the flight dynamics of flexible aircraft using general body axes. *AIAA Journal*, 54(11), 3516–3534.

[8] Albano, E. and Rodden, W. P. (1969). A doublet-lattice method for calculating lift distributions on oscillating surfaces in subsonic flows. *AIAA journal*, 7(2), 279–285.

[9] Eversman, W. and Tewari, A. (1991). Consistent rational-function approximation for unsteady aerodynamics. *Journal of Aircraft*, 28(9), 545–552.

[10] Stevens, B. L., Lewis, F. L., and Johnson, E. N. (2015). *Aircraft control and simulation: dynamics, controls design, and autonomous systems*. John Wiley & Sons.

[11] Apkarian, P. and Noll, D. (2006). Nonsmooth h_infty synthesis. *IEEE Transactions on Automatic Control*, 51(1), 71–86.

[12] Gahinet, P. and Apkarian, P. (2011). Structured h synthesis in matlab. *IFAC Proceedings Volumes*, 44(1), 1435–1440.

[13] László, Á. (2002). On the bounded real lemma. *Systems & control letters*, 45(5), 339–346.

[14] Apkarian, P. and Noll, D. (2015). Optimization-based control design techniques and tools. *Encyclopedia of Systems and Control*, 1001–1011.

[15] Bompart, V., Apkarian, P., and Noll, D. (2007). Non-smooth techniques for stabilizing linear systems. In *American Control Conference, 2007. ACC'07*. IEEE, pp. 1245–1250.

[16] of defense, D. (2008). General specification for flight control systems: design, installation and test of piloted aircraft. Tech. Rep. MIL-DTL-9490E.

[17] Skogestad, S. and Postlethwaite (2005). *Multivariable Feedback Control*. Wiley & Sons.

[18] Lhachemi, H., Saussie, D., and Zhu, G. (2014). A robust and self-scheduled longitudinal flight control system: a multi-model and structured h-infinity approach. In *AIAA Guidance, Navigation, and Control Conference*. p. 0601.

[19] Rugh, W. J. and Shamma, J. S. (2000). Research on gain scheduling. *Automatica*, 36(10), 1401–1425.

COPYRIGHT STATEMENT